Atmos. Chem. Phys. Discuss., 14, 4051–4087, 2014
www.atmos-chem-phys-discuss.net/14/4051/2014/
doi:10.5194/acpd-14-4051-2014

Atmospheric Chemistry and Physics Discussions

Validation of OMI total ozone retrievals from the SAO ozone profile algorithm and three operational algorithms with Brewer measurements

J. Bak[1], X. Liu[2], J. H. Kim[1], K. Chance[2], and D. P. Haffner[3]

[1]Pusan National University, Busan, Korea
[2]Harvard–Smithsonian Center for Astrophysics, Cambridge, MA, USA
[3]Science Systems and Applications, Inc., 10210 Greenbelt Rd, Lanham, MD 20706, USA

Received: 15 November 2013 – Accepted: 5 February 2014 – Published: 14 February 2014

Correspondence to: J. H. Kim (jaekim@pusan.ac.kr)

Published by Copernicus Publications on behalf of the European Geosciences Union.

Abstract

The accuracy of total ozone computed from the Smithsonian Astrophysical Observatory (SAO) optimal estimation (OE) ozone profile algorithm (SOE) applied to the Ozone Monitoring Instrument (OMI) is assessed through comparisons with ground-based Brewer spectrometer measurements from 2005 to 2008. We also make comparisons with the three OMI operational ozone products, derived from the NASA Total Ozone Mapping Spectrometer (TOMS), KNMI Differential Optical Absorption Spectroscopy (DOAS), and KNMI OE (KOE) algorithms. Excellent agreement is observed between SAO and Brewer, with a mean difference of less than ±1 % at most individual stations. The KNMI OE algorithm systematically overestimates Brewer total ozone by 2 % at low/mid latitudes and 5 % at high latitudes while the TOMS and DOAS algorithms underestimate it by ∼ 1.65 % on average. Standard deviations of ∼ 1.8 % are found for both SOE and TOMS, but DOAS and KOE have scatters of 2.2 % and 2.6 %, respectively. The stability of the SOE algorithm is found to have insignificant dependence on viewing geometry, cloud parameters, total ozone column. In comparison, the KOE differences to Brewer values are significantly correlated with solar and viewing zenith angles, with a significant deviation depending on cloud parameters and total ozone amount. The TOMS algorithm exhibits similar stability to SOE with respect to viewing geometry and total column ozone, but stronger cloud parameter dependence. The dependence of DOAS on the algorithmic variables is marginal compared to KOE, but distinct compared to the SOE and TOMS algorithms. Comparisons of All four OMI products with Brewer show no apparent long-term drift but a seasonally affected feature, especially for KOE and TOMS. The substantial differences in the KOE vs. SOE algorithm performance cannot be sufficiently explained by the use of soft calibration (in SOE) and the use of different a priori error covariance matrix, but other algorithm details cause larger fitting residuals by a factor of 2–3 for KOE.

ACPD
14, 4051–4087, 2014

1 Introduction

The Dutch–Finnish Ozone Monitoring Instrument (OMI) (Levelt et al., 2006) aboard the NASA Aura satellite was launched on 15 July 2004 to continue the long term record of satellite total ozone measurements initiated in 1970 with the launch of the nadir-sounding Backscatter Ultra-Violet instrument (BUV) aboard the Nimbus-4 spacecraft, followed in 1978 with the launch of the Total Ozone Monitoring Spectrometer (TOMS) and Solar Backscatter Ultraviolet (SBUV) instruments aboard Nimbus-7. There are two independent operational total ozone algorithms applied to OMI measurements to produce the standard OMI total column ozone products, OMTO3 and OMDOAO3, and one standard profile algorithm to produce the ozone vertical profile product, OMO3PR (KOE). The OMTO3 algorithm is based on the well-known TOMS method developed at NASA Goddard Space Flight Center (GSFC) (Bhartia and Wellemeyer, 2002). The algorithms used for OMDOAO3 and OMO3PR take advantage of the spectroscopic capability of the OMI instrument. They were both developed at KNMI in the Netherlands. One is based on Differential Optical Absorption Spectroscopy (DOAS) (Veefkind et al., 2006) and the other on the optimal estimation (OE) inversion technique (van Oss et al., 2001; Kroon et al., 2011). The variety of OMI operational ozone data products offers a good opportunity for comparing the total ozone retrieval performance among the different algorithms and to identify their strengths and shortcomings.

An independent OE-based ozone profile algorithm, called SOE here, was developed at the Smithsonian Astrophysical Observatory (SAO) (Liu et al., 2010a). It was shown with OMI measurements to be capable of capturing tropospheric ozone signals perturbed by convection, biomass burning, anthropogenic pollution and transport of pollution. In subsequent validation studies, good agreement was found between OMI SOE ozone profiles and high resolution ozone profiles made by satellite and ozonesonde (Liu et al., 2010b; Wang et al., 2011). SOE was shown to capture very well the ozone variability in the extratropical tropopause region through comparison with aircraft and ozonesonde measurements (Pittman et al., 2009; Bak et al., 2013).

ACPD
14, 4051–4087, 2014

Liu et al. (2010a) indicated that the total ozone retrieval errors (root sum square of both random noise and smoothing error) from SOE are typically 1–2.0 DU on average at solar zenith angle $< 80^{\circ}$. However, systematic errors due to systematic measurement errors and forward model and model parameter errors were not assessed. In addition, the total ozone retrieval performance has not been evaluated with independent ground-based observations. The main objective of this study is to evaluate the retrieval performance in total ozone through comparison with four years (2005–2008) of Brewer observations over the Northern Hemisphere, collected from Would Ozone and Ultraviolet Radiation Data Centre (WOUDC) network and the Sodanklyä Total Column Ozone Intercomparison (SAUNA) campaign. The dependence of SOE–Brewer differences on various algorithmic variables (solar zenith angle, cross-track position, cloud parameters, total ozone amount) is thoroughly examined to identify possible problems of SOE under certain conditions. SOE total ozone columns are further evaluated for long-term stability and seasonal/daily variability. The evaluation of possible dependence on algorithmic variables and time will provide useful insights into the characteristics of this algorithm, which have not come from previous studies. The same comparison with Brewer measurements has been conducted for the three operational total ozone products for intercomparison against SOE total ozone. Both OMTO3 and OMDOAO3 were validated previously by several groups using various reference data (e.g., Balis et al., 2007; Kroon et al., 2008; McPeters et al., 2008; Antón and Loyola, 2011). However, total ozone from the OMO3PR product has not yet been thoroughly evaluated against ground-based measurements. This study will thus contribute to the assessment of this product. In principle, OE-based profile algorithms should have the potential to provide more accurate total ozone estimates than the two total ozone algorithms because of its use of a wider wavelength range (270–330 nm) than that used for total ozone (Bhartia and Wellemeyer, 2002; Veefkind et al., 2006). However, the successful performance of spectroscopic profile retrieval algorithms can be accomplished only when accurate calibration and forward model simulations and good knowledge of measurement errors and the a priori covariance matrix are available (Liu et al., 2005, 2010a). In this paper,

ACPD
14, 4051–4087, 2014

one of our interests is to see how total ozone retrieval performance differs between SOE and KOE due to the different implementations of OE.

This paper is organized as follows. Section 2 briefly describes the four retrieval algorithms and datasets and the ground-based total ozone data with the comparison methodology. Sections 3 and 4 provide the OMI validation results using WOUDC and SAUNA data, respectively. We discuss the effect of different implementations between SOE and KOE on total column ozone retrievals in Sect. 5. Section 6 summaries our validation results.

2 Data sets and comparison methodology

2.1 Ozone monitoring instrument (OMI) and OMI ozone algorithms

OMI is a nadir viewing, ultraviolet-visible (UV-VIS) spectrometer, measuring backscattered solar radiances and irradiances over a wavelength range of 270 nm to 500 nm with two spectral channels: uV 270–370 nm and VIS 350–500 nm (Levelt et al., 2006). The UV channel is further divided into two sub-channels, UV-1 and UV-2, at about 310 nm, to suppress straylight. OMI provides daily global coverage with an approximately 2600 km wide swath on the ground. Each swath consists of 60 and 30 cross-track pixels for UV-2/VIS and UV-1 spectra, respectively. The ground pixel size at nadir is 24 km (UV-2/VIS) and 48 km (UV-1) in the across-track direction and 13 km in the flight direction.

An OE-based solution corresponds to a weighted average between measurement and a priori information, constrained by measurement and a priori error covariance matrices (Rodgers, 2000). The SAO and KNMI algorithms, SOE and KOE, are both based on the OE method and derive ozone profile information from OMI ultraviolet spectrum with a fitting window of ∼ 270–310 nm from the UV-1 channel and ∼ 310–330 nm from the UV-2 channel. Two adjacent spectral pixels across the track in UV-2 are combined to match the UV-1 spatial resolution. The OMI random-noise errors

ACPD
14, 4051–4087, 2014

from the level 1b data are used to construct the measurement error covariance matrix. Ozone cross sections are from Brion–Daumont–Malicet (BDM) (Brion et al., 1993) which was recommended for use in ozone profile retrievals from UV measurements by Liu et al. (2007) and Liu et al. (2013). Otherwise, the two algorithms have many different implementations including state and a priori components, radiative transfer model calculations, and radiometric and wavelength calibration treatments. Details can be found in Liu et al. (2010a) and Kroon et al. (2011).

The SOE performs a wavelength and across-track dependent soft calibration to OMI level 1b radiances independent of space and time to correct possible calibration errors causing cross-track and wavelength dependent biases and part of the straylight error (Liu et al., 2010a). The a priori information (mean and standard deviation) for ozone is taken from a monthly and latitude dependent ozone profile climatology from McPeters et al. (2007), the "McPeters–Logan–Labow (LLM)" climatology. The retrieval variables ("state vector") include ozone values at 24 layers from the surface to ~ 0.087 hPa, surface albedo, cloud fraction, scaling parameters for the Ring effect, radiance/O_3 cross section wavelength shift, radiance/irradiance wavelength shift, and a scaling parameter for mean fitting residual. The total column ozone is determined by summing up partial ozone columns of all the layers. Stratospheric and tropospheric ozone columns are separated at the tropopause level defined from National Center for Environmental Prediction (NCEP) Global Forecast System (GFS) Final (FNL) operational global analysis data (http://rda.ucar.edu/datasets/ds083.2/). It should be noted that the SOE algorithm used in this study has several updates from the version presented by Liu et al. (2010a), which are described in Kim et al. (2013).

The KOE algorithm does not perform radiometric calibration like the SOE but performs a straylight correction by minimizing the signatures of Fraunhofer features in the fit residual separately in the UV-1 and UV-2 channels. The a priori ozone mean state is defined from LLM climatology, but the a priori ozone error is defined as a constant relative variability, 20 % for all latitudes and altitudes except for ozone hole conditions. The retrieval variables include ozone profiles at 18 layers from the surface to 0.3 hPa,

ACPD
14, 4051–4087, 2014

surface albedo, cloud albedo, and straylight correction parameters. The surface albedo and cloud albedo is turned on or off depending on the cloud fraction as a state vector; for cloud fraction < 0.2 the surface albedo is fitted with fixed cloud albedo of 0.8 whereas for the cloud fraction > 0.2 the cloud albedo is fitted with the fixed surface albedo to its a priori value (Kroon et al., 2011).

The OMI TOMS and OMI DOAS total ozone algorithms use UV-2 measurements and thus retrievals are done at the higher UV-2 spatial resolution. The TOMS algorithm uses sun-normalized radiances at just two wavelengths, 317.6 and 331.3 nm, under most retrieval conditions. One wavelength is significantly absorbed by ozone and sensitive to the total column amount, and the other is insensitive to ozone. The algorithm is rather insensitive to calibration error independent of the wavelengths, but more sensitive to relative error (Bhartia and Wellemeyer, 2002). This algorithm uses ozone cross sections data based on Bass and Paur (1985). So-called "soft calibration" radiometric adjustments determined from analysis of Earth-view data are made to the OMI radiances before applying the TOMS algorithm in order to reduce the dependence on cross-track positions. The DOAS algorithm calculates the slant column density with a DOAS-based fitting of the measured spectrum in the spectral region 331.1–336 nm to the differential absorption cross sections of ozone using BDM cross sections; then, it estimates the vertical column density by dividing the slant column density by the Air Mass Factor (AMF) (Veefkind et al., 2006).

In all four OMI ozone algorithms, clouds are treated as Lambertian reflectors and partially cloudy scenes are treated using the independent pixel approximation or mixed Lambertian surfaces. SOE uses effective cloud top pressure from the OMI O_2-O_2 algorithm (Acarreta et al., 2004), but derives the initial effective cloud fraction from 347 nm and further fits it in the retrieval. TOMS takes the optical centroid pressure (OCP) from the OMI Rotational Raman Cloud Pressure algorithm, OMCLDRR (Joiner and Vasilkov, 2006) and derives the effective cloud fraction from 331.3 nm in most cases. Both KOE and OMDOAO3 use cloud information (effective cloud fraction and cloud-top pressure)

ACPD
14, 4051–4087, 2014

from the OMI O_2-O_2 absorption cloud pressure algorithm, OMCLDO2 (Acarreta et al., 2004).

The OMI ozone standard products are from the Aura Validation Data Centre (AVDC) (http://avdc.gsfc.nasa.gov), which provides the OMI overpass observations over many ground stations. OMTO3 is processed with the TOMS v 8.5 algorithm (Bhartia and Wellemeyer, 2002) and OMDOAO3 is processed with the DOAS v 1.2.3.1 algorithm (Veefkind et al., 2006). Both OMTO3 and OMDOAO3 are retrieved for individual UV-2 pixels. The KOE data used in this study were processed with v 1.1.0 before 2 January 2006 and with v 1.1.1 since then (van Oss et al., 2001; Kroon et al., 2011). The KOE product is retrieved for 1 out of 5 UV-1 pixels along-track (i.e., retrieves for 1 UV1 pixel, then skips 4 pixels) (http://disc.sci.gsfc.nasa.gov/Aura/data-holdings/OMI/documents/v003/OMO3PRO_README.html). For SOE, we selectively conduct retrievals at the locations of KOE products which are collocated with Brewer measurements. It is reported that the effective cloud fraction is not written correctly to the output for values larger than 0.2 in the KOE v 1.1.0 algorithm. Therefore, we replace cloud fraction values larger than 0.2 for KOE data before 2 January 2006 with the output of the SOE algorithm. Because the OE retrievals have coarser resolution (UV-1 vs. UV-2) and skip pixels along the track, they are on average less collocated (more distant) from ground measurements.

2.2 WOUDC total ozone data

The Brewer grating spectrometer has an improved optical design over the Dobson spectrometer and is fully automated. The Brewer can be operated in single or double monochromator configuration. The double monochromator (MK-III model) is known to better reduce the impact of straylight on the measurement than the single monochromator (MK-II or MK-IV) does (Kerr, 2002; Petropavlovskikh et al., 2011). Spectral irradiance measurements can be made by a well-maintained Brewer instrument with the precision of $\sim \pm 0.1$ % (Kerr, 2002). It measures spectral irradiance at six wavelengths ranging from 303.2 to 320.1 nm. The Brewer measurement at 303.2 nm is only used

ACPD
14, 4051–4087, 2014

to check the spectral wavelengths by means of internal Hg lamps. The channel at 305.3 nm is used to retrieve the sulfur dioxide (SO_2) column and the ozone column is retrieved from a combination of five longer wavelengths (306.3, 310.1, 313.5, 315.8, and 320.1 nm) (Schneider et al., 2008). Absorption cross coefficients based on Bass and Paur (1985) data are used in Brewer operation algorithms. There could be a systematic bias in total ozone calculations due to switching to other cross sections from Bass–Paur cross section (Redondas et al., 2013); for example, this may have an impact as large as −3.2 % if the BDM cross-sections are used. The temperature dependence of the ozone absorption coefficients can be a problem because ozone cross section at a fixed temperature of the ozone layer (228.2 K for Brewer calculations, 226.9 K for Dobson calculations) is applied in the standard retrieval unlike in the satellite retrievals. Kerr (2002) found less temperature dependence at the Brewer wavelengths (0.094 %$^\circ C^{-1}$) than at the Dobson wavelengths (1.3 %$^\circ C^{-1}$). Therefore, a better agreement has been typically reported in the comparison of satellite measurements with Brewer measurements than with Dobson measurements (e.g., Weber et al., 2005; Koukouli et al., 2012). We use daily mean values derived from Brewer spectrometers that are publicly available from the World Ozone and Ultraviolet Radiation Data Centre (WOUDC) archive (http://woudc.org) because hourly data are available for every year from 2005 to 2008 for only 10 stations. Daily mean values are reported as the average of all direct sun (DS) measurements during the course of day if one or more DS observations are available. Otherwise, the daily mean values are derived from other types of measurements, mostly from zenith sky (ZS) observations. This study only considers the DS measurements, to ensure the most reliable accuracy. Thirty-six stations, listed in Table 1, have been initially selected from the WOUDC archive to be used for OMI validation. These stations have at least 100 days with DS measurements every year. Five stations are equipped with double Brewer instruments and the rest with single Brewer instruments; Uccle (50.8° N, 4.35° E) provides both single and double Brewer measurements.

ACPD
14, 4051–4087, 2014

2.3 SAUNA campaign total ozone data

The main objective of the Sodankylä Total Column Ozone Intercomparison (SAUNA) campaign was to assess the performance of the ground-based instruments and algorithms which measure total column ozone at large solar zenith angles and high total column ozone amounts (http://fmiarc.fmi.fi/SAUNA/). The SAUNA campaign was held in Sodankylä, Finland, located 120 km north of the Arctic Circle, in March/April of 2006. The early springtime at this high latitude provides the ideal large solar zenith angles for the mission, and total ozone is consistently higher than 400 DU over Sodankylä at this time of year. The ground-based total ozone data were collected in near real time, within 24 h from single/double Brewer and Dobson instruments, including several regional and world standard instruments. The total ozone reference for the SAUNA campaign from Brewer measurements combining direct sun data from 5 instruments, double Brewers #185, #171, and #085, and single Brewers #037 and #039 is used in this validation work. The SAUNA data were not averaged daily for comparison; we use the individual observations closest to OMI overpass time.

2.4 Comparison methodology

A portion of the OMI radiance measurements are affected by an instrument error termed the "row-anomaly" which began in June of 2007. Loose thermal insulating material in front of the instrument's entrance slit is believed to both block and scatter light, causing measurement error. The anomaly affects radiance measurements at all wavelengths for specific cross-track viewing directions which are imaged to the CCD rows. Initially, the anomaly only affected a few rows (2 positions in 2007, 8 positions starting from 11 May 2008). But, since January 2009, the anomaly spread to other rows and began to shift with time. While a large fraction of good measurements remain in the UV-2 and VIS channels used by OMTO3 and OMDOAO3, the effect of the anomaly on UV-1 measurements used by the SOE and KOE algorithms is widespread and severe.

ACPD
14, 4051–4087, 2014

Therefore in this study, OMI data are only used from the period of 2005–2008 when the row anomaly did not substantially affect radiance data used by the four algorithms.

The criteria for collocating OMI with Brewer data are within 150 km between OMI pixel center and ground-based station location and on the same day. We take only the closest match on a given day, not the average of OMI pixels found. The location and overpass time of KOE and SOE (and, separately, of TOMS and DOAS) collocated at one ground point are exactly the same whereas the locations differ slightly between SOE/KOE and TOMS/DOAS. The average distance between OMI and the ground stations is 1 ± 6 km for OMTO3 and OMDOAO3 products and 30 ± 14 km for KOE and SOE products. For simultaneous evaluation of four total ozone columns as a function of cross-track position, the cross-track position of UV-2 is remapped into positions across the track for UV-1 (e.g., 1–2 of UV-2 corresponds to 1 of UV-1; 3–4 of UV-2 corresponds to 2 of UV-1).

Two statistical quantities, mean bias and 1σ standard deviation, are calculated from relative differences between OMI and Brewer total ozone columns, defined as $\frac{\mathrm{OMI}_i - \mathrm{Brewer}_i}{\mathrm{Brewer}_i} \cdot 100$. Note that relative differences derived under extreme conditions such as solar zenith angles $> 80^\circ$, cloud fractions > 0.8, and Aerosol Index values > 2 and the outliers (outside 3σ of the mean value) are excluded. The mean bias and 1σ standard deviation are presented for individual stations in Sect. 3.1. In Sects. 3.2 to 3.6 we have merged all collocated OMI and WOUDC datasets to examine the possible dependency of OMI/Brewer differences on OMI viewing geometries, cloud parameters, total ozone amount, and time.

3 Comparison results between OMI and WOUDC data

3.1 Comparison at individual stations

There are 36 stations available from the WOUDC archive for this validation study, as mentioned in Sect. 2.2. 29 Brewer stations among them were identified as a good

ACPD
14, 4051–4087, 2014

references using a similar selection procedure as that used by Balis et al. (2007). This selection procedure is described in the rest of this section.

Figure 1 shows the relative differences between OMI and Brewer total ozone at all 36 stations listed in Table 1. On average, both mean biases and 1σ standard deviations show smooth variation from station to station with exceptions at Pohang (36.03° N, 129.38° E), Mt. Waliguan (36.29° N, 100.9° E), and Alert (82.45° N, 62.51° W). A larger positive bias detected at Mt. Waliguan (elevation: 3820 nm) could arise from the discrepancy between the actual station elevation and the average altitude of OMI ground pixels. The overall standard deviation values range from 1.5 % to 2.5 %, except for Pohang and Alert, where they exceed 3 %. This deviation could be caused by problems with ground-based data rather than with satellite data because satellite measurement characteristics are changing slowly (Floletov et al., 2008). In addition, a large standard deviation at Alert could be attributed to uncertainties in the retrieval of ozone columns from satellite UV/VIS measurements at high solar zenith angles.

Among the four algorithms, the SOE data present the best agreement with Brewer data at most stations; the mean difference is typically below ±1 %. TOMS and DOAS results present similar negative biases at tropical mid-latitude stations, but DOAS biases are slightly smaller than TOMS at high latitude stations. The worst agreement is found for KOE total ozone retrievals at all stations. The KOE data persistently overestimate Brewer total ozone measurements, with average biases of ∼ 2 % at latitudes below 43° up to ∼ 5 % at high latitudes. Other OMI data, when they deviate, typically underestimate. The SOE and TOMS comparisons show similar standard deviations of 1.8 % on average. The DOAS comparison shows larger values, between 2 % and 2.5 %. The KOE-Brewer differences have the largest scatter at most stations, with standard deviations up to 3 %.

We examine the correlations between OMI and Brewer data in left panel of Fig. 2. Two tropical stations (Paramaribo and Petaling Jaya) are excluded from comparisons because of their small correlation coefficients compared to the overall values of other stations. In addition, the Pohang, Mt. Waliguan, and Alert stations, where the mean

ACPD
14, 4051–4087, 2014

differences deviate highly, show inconsistencies from neighbouring stations. Apart from these stations, the comparisons present high correlation coefficient values, between 0.95 and 1, depending on OMI algorithms and stations. The SOE and TOMS total ozone columns show the best correlations with Brewer data ($R \sim 0.99$). The KOE data shows the smallest correlations at most stations.

We derive the trend (% yr^{-1}) using the linear regression slope of four years of the monthly averaged relative differences shown as a function of station in the right panel of Fig. 2. As a result of this trend analysis, we exclude three stations from comparisons, Marcus Island, Rome, and Edmonton where all OMI retrievals show absolute trends of more than 0.4 % yr^{-1}.

Finally, 29 stations are selected as good references to be used for the validation of OMI total column ozone data sets. Comparison statistics are in Table 2. For all stations in the Northern Hemisphere (NH), the average difference between SOE and Brewer is 0.02 % (0.04 DU) with a standard deviation of 1.81 % (5.98 DU), which generally represents an improvement over other comparisons presented in this study as well as in previous validation studies for other space-borne instruments (e.g., Antón and Loyola, 2011; Koukouli et al., 2012). Overall, the SOE algorithm also demonstrates the best agreement with Brewer among all four algorithms with respect to correlation coefficients and linear regression results for the NH, middle latitude and high latitude regions. Despite the use of only two wavelengths, the TOMS algorithm shows similar standard deviations to the SOE algorithm (slightly smaller at mid-latitude stations, but slightly larger at high latitude stations) except for larger biases of −1.70 %. A slightly larger scatter of SOE comparison (1.79 %) against that of TOMS (1.76 %) observed in mid-latitudes could be attributed to SOE's further distance from ground stations rather than the algorithm performance. We have examined how the SOE–Brewer standard deviations change when SOE total ozone is retrieved at locations of TOMS measurements: they are reduced to 1.71 % in mid-latitudes and 1.78 % in high latitude, which is less scatter than TOMS. The NH mean difference between DOAS and Brewer is -1.59 ± 2.18 % and between KOE and Brewer 2.76 ± 2.60 %. Compared to SOE and

ACPD
14, 4051–4087, 2014

TOMS, both DOAS and KOE show larger differences in mean biases between middle and high latitudes. These are related to the solar zenith angle dependence as discussed in the following Section.

3.2 Solar zenith angle dependence

The solar zenith angle (SZA) of polar orbiting satellite changes dramatically from the tropics to the poles as well as seasonally from summer to winter. Tropospheric ozone information available from satellite UV measurements decreases at larger SZA (Liu et al., 2005) and radiative transfer simulations lose accuracy for very high SZA (Caudill et al., 1997). The possible dependence of retrieval algorithms on SZA can cause seasonal/latitudinal dependent retrieval biases. In Fig. 3a, the stability of each algorithm is assessed for SZA dependency between 20° and 80° (5° bins). The SOE and TOMS algorithms have a slight dependence on SZA, mean relative differences being increase (or decrease) within 1 % over all bins. The DOAS differences show obvious dependence ranging from −2.2 % at SZA 22.5° to −0.6 at SZA 77.5° (i.e., bias change by 1.6 % or 5.3 DU), but the SZA dependence of this product processed with v 1.2.3.1 of the DOAS algorithm from collection 3 OMI level-1b data is significantly improved over the previous data version. For example, increasing mean biases of more than 2 % due to SZA were found in OMDOAO3 (v 1.0.5, collection 3)–Brewer data (Koukouli et al., 2012) and the OMDOAO3 collection 2 product showed a much stronger SZA dependence by ∼ 4 % (Balis et al., 2007; McPeters et al., 2008). The overestimation of the KOE algorithm is negatively correlated with SZA bins below 60°, but positively correlated for larger SZA bins.

As indicated in Koelemeijer and Stammes (1999) and Antón and Loyola (2011), it is important to evaluate the joint effects of satellite viewing geometries and clouds on ozone retrievals. In Fig. 4, the SZA dependence is characterized by sub-groups of cloud fraction and OMI cross-track positions, respectively. This outcome demonstrates again the stable performance of the SOE algorithm. On the other hand, the SZA dependence of OMI–Brewer differences derived from other algorithms is changed due to

ACPD
14, 4051–4087, 2014

cloud fraction, especially at SZA bins below 60°. The SZA dependence of the DOAS algorithm becomes more evident with cloudiness, which is a usual characteristic of the total column ozone data based on the DOAS technique (Antón and Loyola, 2011). The negative SZA dependence of the TOMS algorithm also becomes apparent for cloudy conditions. In contrast, KOE presents a larger SZA dependence for clear-sky conditions. For high SZAs (> 6°) the SZA dependence is similar between high and low cloud fraction groups, which is a common characteristic of all OMI ozone algorithms. Moreover, the SZA dependence for the DOAS algorithm is larger at nadir positions than at the off-nadir positions. A systematic offset of 1 % between nadir and the off-nadir positions is present in KOE differences for the whole SZA range, but the SZA dependence shows little dependence on cross-track positions. The SZA dependence of the TOMS algorithm is not affected by the OMI cross-track position.

3.3 Cross-track position dependence

The OMI swath contains 30 and 60 cross-track pixels for the UV-1 and UV-2 channels, respectively. The viewing angles ranges from near 0° at nadir to almost 70° at the extreme off-nadir position. In addition, OMI uses CCD detectors, so each cross-track position is essentially measured with a different detector. Liu et al. (2010a) found that the structures of the differences between OMI observations and simulations in the spectral range 270–350 nm depends remarkably on the cross-track position, especially at wavelengths shorter than 310 nm. Most of the OMI products are reported to have cross-track dependent biases or striping. Therefore, the performance of the OMI level 2 algorithms should be assessed with respect to the cross-track position.

The dependence of OMI/Brewer biases on cross-track position is examined in Fig. 3b. It shows strong cross-track dependence in the KOE data, with the maximum biases of ∼ 4 % at nadir and the minimum biases of ∼ 1 % at extreme off-nadir positions. The smooth variation with cross-track position may indicate errors in the forward model simulations. The overall relative differences over all cross-track positions are ∼ −2 % in both DOAS and TOMS comparisons. However, the DOAS relative differences fluctuate

ACPD
14, 4051–4087, 2014

considerably with cross-track positions, especially at the 4, 16, 20, and 26 positions, where the mean bias deviates significantly from the average value (−2 %) by up to ∼ ±1 % or more. To our knowledge, the DOAS and KOE algorithms do not apply any additional correction to OMI level 1b data. On the other hand, both TOMS and SOE algorithms apply a correction to OMI radiance measurements to remove cross-track variability, which may result in less dependence on cross-track position in the comparison with Brewer data. In Sect. 5, we will show the effect of soft calibration on SOE–Brewer differences to see whether this calibration can explain the large difference in the dependence on cross-track position between SOE and KOE algorithms.

3.4 Cloud parameter dependence

The effect of clouds on trace-gas retrievals from satellite observations is well established in the literature (Antón and Loyola, 2011). OMI ozone algorithms use a Lambertian surface model for a cloud with a fixed albedo of 0.8, requiring the effective cloud-top pressure (or optical centroid pressure) and effective cloud fraction to model the cloud. The accuracy of ozone retrievals is sensitive to the uncertainties of cloud information and cloud treatment and therefore the validation results should be examined with respect to cloud parameters used in retrieval algorithms (Koelemeijer and Stammes, 1999; Antón and Loyola, 2011). It was shown in Sect. 3.1 that the effect of cloudiness on validation results becomes more evident for smaller SZAs. Therefore, in order to clearly investigate the effect of clouds on the comparison, we show relative differences with SZAs smaller than 45° as a function of cloud parameters in Fig. 3c and d.

Figure 3c shows the influence of cloud fraction on the OMI-Brewer comparisons. The DOAS and TOMS results present similar negative and stable biases for cloud fraction bins less than ∼ 0.3, but the difference between DOAS and TOMS biases becomes larger with increasing cloudiness because of their opposite dependency on the cloud fraction. The DOAS biases increase negatively from −1.5 % for low cloud fraction bins up to −2.5 % for high cloud fraction bins, while the TOMS biases increase posi-

ACPD
14, 4051–4087, 2014

tively within 1 %. The KOE biases are larger under partly cloudy conditions (0.2 < cloud fraction < 0.8) relative to under clear-sky and overcast conditions, which could be related to a switch point in the algorithm between fitting the surface albedo and fitting the cloud albedo (J. P. Veefkind, personal communication, 2013). The SOE algorithm shows a remarkable stability for both clear and cloudy conditions with the mean biases within ±0.5 % except for the bin of 0.95–1.0 where the mean bias is around −1.5 %. The standard deviations of the relative differences persistently increase with increasing cloudiness for all four OMI algorithms.

Figure 3d shows the influence of the cloud top pressure on the OMI-Brewer comparisons. All the four algorithms show no significant dependence on cloud-top pressure except for high clouds (cloud top pressure <∼ 350 hPa), the average OMI–Brewer differences are larger by 1–2 % than those for middle and low clouds. Of all the four algorithms, the SOE algorithm shows the least dependence on cloud-top pressure. The standard deviations increase smoothly from low to high clouds except for TOMS where the standard deviations increase rapidly from 325 hPa to 275 hPa.

3.5 Total ozone column dependence

In Fig. 3e the differences between OMI and Brewer measurements are plotted as a function of Brewer total ozone column in bins of 25 DU. The dependence on the total column ozone could be attributed to the sensitivity to profile shape of retrieved total ozone at high SZAs due to the difference between actual and assumed a priori (climatological) ozone profiles as indicated by Lamsal et al. (2007) and Antón et al. (2009). There is ∼ 2 % difference of DOAS mean biases between low (< 325 DU) and high ozone amounts (> 425 DU). This behaviour could be explained partially by the positive dependence of the DOAS algorithm on SZA because high ozone values usually occur at high latitudes where SZAs are large. The KOE mean biases generally decrease from ∼ 3 % at low values to ∼ 1 % at high values and its standard deviations show a deviation of 2.5 to 3.5 % whereas other comparisons have a standard deviation of ∼ 2 % over all the given bins. SOE and TOMS comparisons have much smoother total ozone depen-

ACPD
14, 4051–4087, 2014

dence. TOMS mean biases range from −2.1 % to −1.3 % and SOE mean biases are below ±0.4 % over all the given bins except at the lowest total ozone value where the mean bias is ∼1 %. Using the improved tropopause-based ozone profile climatology presented by Bak et al. (2013) in the SOE algorithm further slightly reduces the total ozone dependence in both mean biases at low ozone amounts and standard deviations at high ozone amounts (see the red dashed line in Fig. 3e).

3.6 Seasonal dependence

We examine the long-term stability and seasonal variation of the OMI total column ozone retrievals to evaluate the four OMI algorithms. Figure 5 shows the four year time series of the total ozone relative differences in four latitude ranges between 30° N and 80° N. The blue line indicates the linear regression of monthly relative differences. None of the algorithms shows significant long-term drift in OMI-brewer comparisons, except for the KOE algorithm at 50–58° N, when the trend is 0.31 % yr^{-1}. The monthly mean biases of the SOE–Brewer differences vary around the annual means within ±0.4 % and their seasonal dependence is quite small for the three latitude bands below 60° N. However, monthly mean biases at the high latitude band (64–79° N) show a clear seasonal-dependent signature with a maximum in winter and a minimum in summer. A similar seasonal-dependent pattern is observed in the monthly mean biases of DOAS for all latitude bands, with a quite high correlation between DOAS and SOE temporal variations of the monthly mean biases, ranging from 0.70 and 0.89 (Table 3). For the two low-latitude bands, time series of the monthly mean differences between KOE and Brewer show a distinct annual variation with a winter minimum bias of −1 % and a summer maximum bias of ∼ 3.5 %, which is negatively correlated with the seasonal variation of SZA (Table 3; R = −0.66 to −0.81). This behaviour could be explained by the negative dependence of KOE biases detected at small SZAs as shown in Fig. 4a. In contrast, there is negligible (positive) correlation between the seasonal variation and SZA for the two high-latitude bands. TOMS monthly mean biases have a seasonal-dependent pattern of a winter minimum bias and a summer maximum bias at two

ACPD
14, 4051–4087, 2014

latitude bands between 40° N and 58° N where biases and SZAs is correlated with a coefficient of −0.54 to −0.65.

4 Comparison between OMI and SAUNA data

Figure 6 compares the daily time series of total ozone columns from OMI and SAUNA Brewer measurements at Sodanklyä for April 2006 when solar zenith angles are above 50°. The Brewer measurements show large daily variability, which is in good agreement with OMI total ozone variations. The KOE total ozone is positively biased relative to SAUNA data with the largest standard deviation. Both TOMS and DOAS are negatively biased by more than 2 %, with TOMS–SAUNA having largest mean bias and smallest standard deviation. The SOE-SAUNA differences are negatively biased with the smallest mean bias among the comparisons and a slightly larger scatter than TOMS-SAUNA differences. This scatter of SOE differences is reduced to 3.6 DU when SOE retrievals are done at the locations of TOMS products. The comparison with SUANA data is generally consistent with results found in the comparison between OMI and WOUDC at high latitudes.

5 Comparison between SAO and KNMI OE ozone profile algorithms

Although the SOE and KOE algorithms are similar, the SOE algorithm shows significantly better performance in retrieved total ozone. Two of the major algorithmic differences are the use of soft calibration and the use of a priori error from the LLM climatology (vs. 20 % throughout the atmosphere) in the SOE algorithm. In order to investigate whether the retrieval performance differences between two algorithms are caused by these two algorithmic differences, we perform SOE retrieval experiments with modified implementations corresponding to KOE. First, we retrieve total ozone columns using the SAO algorithm with and without soft calibration and then compare both retrievals

ACPD
14, 4051–4087, 2014

with Brewer measurements as a function of SZA and cross-track position in Fig. 7. The use of soft calibration slightly reduces the standard deviations, SZA dependence, and cross-track dependence for most positions except for large reductions in mean biases by up to 2 % for the first two positions (UV-1 position 2 and 3). Comparing the magnitudes and patterns in the reductions vs. KOE/SOE differences in Fig. 3a and b, the KOE cross-track dependence at the left side of the OMI swath could be explained by the soft calibration, but the larger SZA and cross-track dependence (nadir to right off-nadir) could not be explained.

Secondly, we examine the effect of using a 20 % relative a priori error on SAO total column ozone retrievals and found no significant differences with total column ozone retrievals based on the LLM a priori error (results not shown here). Therefore, the large KOE/SOE differences are mainly caused by other implantation details such as radiative transfer simulations and fitting of variables other than ozone, which should cause differences in fitting residuals.

Figure 8 compares the average fitting residuals in UV-1 and UV-2 channels for an orbit of retrievals on 1 June 2006 using SOE and KOE, as a function of SZA. For the SAO fitting results shown in Fig. 8b, we turned off the soft calibration and the use of common mode. Both SOE and KOE fitting residuals show the strong SZA dependence, but SAO is smaller by a factor of 2–3. Moreover, the use of soft calibration in SAO algorithm leads to a much larger differences in fitting results between two algorithms, especially in UV-2, where total and tropospheric ozone information originates mostly, by a factor of 2 (at larger SZAs) to 5 (at smaller SZAs) as shown in Fig. 8d and e. This implies significant differences in the retrieved total and tropospheric ozone columns between two algorithms. In addition, the KOE fitting residuals in both UV-1 and UV-2 channels show a peak at SZAs of $\sim 20^{\circ}$ which are contaminated by sun glint (black symbols), whereas the impact of sun glint on the SAO fitting residuals is not apparent even without soft calibration.

ACPD
14, 4051–4087, 2014

6 Conclusions

The OMI total column ozone data processed with SOE and the three OMI operational algorithms (KOE, TOMS, and DOAS) are evaluated using four years (2005–2008) of Brewer measurements at 29 stations identified as good references using a selection procedure similar to that of Balis et al. (2007). The agreement between SOE and Brewer is within ±1 % at most stations; the overall difference is 0.02 % with a standard deviation of 1.81 % over the NH. The TOMS and DOAS comparisons with Brewer have the similar negative biases of ∼ −1.75 % at mid-latitude, but of −1.65 % and −1.22 %, respectively, at high latitude. The KOE algorithm overestimates Brewer total ozone by from ∼ 2 % at mid-latitude to ∼ 5 % at high latitude stations. The standard deviations of KOE and DOAS biases are larger than 2 %. Those of TOMS and SOE biases are ∼ 1.8 % over the NH, but TOMS differences have a slightly less scatter than SOE differences at mid latitude stations. The standard deviations of SOE biases (SOE total ozone is retrieved at the locations of KOE product) could be smaller than TOMS if SOE total ozone is retrieved at the locations of TOMS product. Each SOE and TOMS based total ozone columns show much better correlation with Brewer data than KOE at most stations. The correlation coefficient of DOAS with Brewer is better than those of KOE, but worse than those of SOE and TOMS.

The SOE improvements to total ozone retrievals are distinct, with insignificant dependence of total ozone differences on various algorithmic variables; even the SZA dependence is unaffected by both cloud fraction and cross-track position. However, the SOE biases show significant deviation at high altitude cloud of ∼ 300 hPa, at high cloud fraction of ∼ 0.9, and at low ozone amount of ∼ 250 DU. The dependence of the TOMS algorithm on viewing geometry is generally marginal, but the SZA dependence is enhanced under cloudy conditions. The DOAS algorithm has a positive dependence on SZA, which becomes more significant for cloudy conditions and for large cross-track positions. KOE biases increase negatively (positively) at SZAs smaller (larger) than 60° and depend strongly on the cross-track position with a bias varying between ∼ 1 % and

ACPD
14, 4051–4087, 2014

~ 4 %. The deviation of mean biases for high clouds compared to low and mid-altitude clouds is commonly found in all four OMI comparisons, but with the smallest deviations in the comparison of SOE with Brewer. The positive (negative) correlation is found between TOMS (DOAS) mean biases and cloud fraction. KOE biases are larger at cloud fraction between 0.2 and 0.8 compared to at other cloud fraction values. The SOE and TOMS algorithms exhibit a similar weaker dependence on total ozone amount compared to DOAS and KOE.

A high correlation between SOE and DOAS monthly biases is identified. The common features of their seasonal-dependent errors are a weak seasonal variation in mid-latitude bands and a distinct seasonal variation in high latitude with winter maximum biases and summer minimum biases. The KOE monthly biases have significant seasonal variability for all latitude bands and their seasonal dependences are highly correlated with the features of SZA dependent biases at mid-latitudes. A comparable seasonal variability is found in TOMS differences at mid-latitudes. A comparison with the SAUNA campaign data shows that all four OMI total ozone columns well represent the daily total ozone variations.

Finally, we demonstrated that the use of SAO soft calibration reduces the SZA and cross-track dependences of OMI-Brewer differences and fitting residuals, especially in UV-1 at smaller SZA angles. However, this reduction cannot explain all of the differences in total ozone retrieval performance between the KOE and SOE algorithms. The use of different a priori error covariance matrices is immaterial to the retrieved total ozone. Other differing algorithm details, including radiative transfer simulations and fitting of variables other than ozone, cause significantly larger fitting residuals for KOE by a factor of 2–3.

Acknowledgements. The Brewer ozone data used in this study were obtained though the WOUDC and SAUNA archive. The authors would like to thank OMI science team for providing the satellite data and Pepijn Veefkind and MariLiza Koukouli for providing useful comments regarding the validation results. This research was supported by the Eco Innovation Program of KEITI (ARQ201204015), South Korea. Research at the Smithsonian Astrophysical Observatory was funded by NASA and the Smithsonian Institution.

ACPD
14, 4051–4087, 2014

References

Acarreta, J. R., De Haan, J. F., and Stammes, P.: Cloud pressure retrieval using the O_2–O_2 absorption band at 477 nm, J. Geophys. Res., 109, D05204, doi:10.1029/2003JD003915, 2004.

Antón, M. and Loyola, D.: Influence of cloud properties on satellite total ozone observations, J. Geophys. Res., 116, D03208, doi:10.1029/2010JD014780, 2011.

Antón, M., Loyola, D., López, M., Vilaplana, J. M., Bañón, M., Zimmer, W., and Serrano, A.: Comparison of GOME-2/MetOp total ozone data with Brewer spectroradiometer data over the Iberian Peninsula, Ann. Geophys., 27, 1377–1386, doi:10.5194/angeo-27-1377-2009, 2009.

Bak, J., Liu, X., Wei, J. C., Pan, L. L., Chance, K., and Kim, J. H.: Improvement of OMI ozone profile retrievals in the upper troposphere and lower stratosphere by the use of a tropopause-based ozone profile climatology, Atmos. Meas. Tech., 6, 2239–2254, doi:10.5194/amt-6-2239-2013, 2013.

Balis, D., Kroon, M., Koukouli, M. E., Brinksma, E. J., Labow, G., Veefkind, J. P., and McPeters, R. D.: Validation of Ozone Monitoring Instrument total ozone column measurements using Brewer and Dobson spectrophotometer ground-based observations, J. Geophys. Res., 112, D24S46, doi:10.1029/2007JD008796, 2007.

Bass, A. M. and Paur, R. J.: The ultraviolet cross-sections of ozone, I, The measurements, in: Atmospheric Ozone, edited by: Zerefos, C. S., Ghazi, A., and Reidel, D., Norwell, Mass., 606–610, 1985.

Bhartia, P. K. and Wellemeyer, C.: TOMS-V8 total O3 algorithm, in: OMI Algorithm Theoretical Basis Document, Vol. II, OMI Ozone Products, edited by: Bhartia, P. K., 15–31, NASA Goddard Space Flight Cent., Greenbelt, MD, 2002.

Brion, J., Chakir, A., Daumont, D., and Malicet, J.: High-resolution laboratory absorption cross section of O3. Temperature effect, Chem. Phys. Lett., 213, 610–512, 1993.

Caudill, T. R., Flittner, D. E., Herman, B. M., Torres, O., and McPeters, R. D.: Evaluation of the pseudo-spherical approximation for backscattered ultraviolet radiances and ozone retrieval, J. Geophys. Res., 102, 3881–3890, 1997.

Joiner, J. and Vasilkov, A. P.: First results from the OMI rotational Raman scattering cloud pressure algorithm, IEEE T. Geosci. Remote, 44, 1272–1282, 2006.

ACPD
14, 4051–4087, 2014

Kerr, J.: New methodology for deriving total ozone and other atmospheric variables from Brewer spectrophotometer direct sun spectra, J. Geophys. Res., 107, 4731, 2002.

Kim, P. S., Jacob, D. J., Liu, X., Warner, J. X., Yang, K., Chance, K., Thouret, V., and Nedelec, P.: Global ozone–CO correlations from OMI and AIRS: constraints on tropospheric ozone sources, Atmos. Chem. Phys., 13, 9321–9335, doi:10.5194/acp-13-9321-2013, 2013.

Koelemeijer, R. B. A. and Stammes, P.: Effects of clouds on ozone column retrieval from GOME UV measurements, J. Geophys. Res., 104, 8281–8294, doi:10.1029/1999JD900012, 1999.

Koukouli, M. E., Balis, D. S., Loyola, D., Valks, P., Zimmer, W., Hao, N., Lambert, J.-C., Van Roozendael, M., Lerot, C., and Spurr, R. J. D.: Geophysical validation and long-term consistency between GOME-2/MetOp-A total ozone column and measurements from the sensors GOME/ERS-2, SCIAMACHY/ENVISAT and OMI/Aura, Atmos. Meas. Tech., 5, 2169–2181, doi:10.5194/amt-5-2169-2012, 2012.

Kroon, M., Petropavlovskikh, I., Shetter, R., Hall, S., Ullmann, K., Veefkind, J. P., McPeters, R. D., Browell, E. V., and Levelt, P. F.: OMI total ozone column validation with Aura-AVE CAFS observations, J. Geophys. Res., 113, D15S13, doi:10.1029/2007JD008795, 2008.

Kroon, M., de Haan, J. F., Veefkind, J. P., Froidevaux, L., Wang, R., Kivi, R., and Hakkarainen, J. J.: Validation of operational ozone profiles from the Ozone Monitoring Instrument, J. Geophys. Res., 116, D18305, doi:10.1029/2010JD015100, 2011.

Lamsal, L. N., Weber, M., Labow, G., and Burrows, J. P.: Influence of ozone and temperature climatology on the accuracy of satellite total ozone retrieval, J. Geophys. Res., 112, D02302, doi:10.1029/2005JD006865, 2007.

Levelt, P. F., van den Oord, G. H. J., Dobber, M. R., Malkki, A., Visser, H., de Vries, J., Stammes, P., Lundell, J. O. V., and Saari, H.: The Ozone Monitoring Instrument, IEEE T. Geosci. Remote, 44, 1093–1101, doi:10.1109/TGRS.2006.872333, 2006.

Liu, C., Liu, X, and Chance, K.: The impact of using different ozone cross sections on ozone profile retrievals from OMI UV measurements, J. Quant. Spectrosc. Ra., 130, 365–372, doi:10.1016/j.jqsrt.2013.06.006, 2013.

Liu, X., Chance, K., Sioris, C. E., Spurr, R. J. D., Kurosu, T. P., Martin, R. V., and Newchurch, M. J.: Ozone profile and tropospheric ozone retrievals from Global Ozone Monitoring Experiment: algorithm description and validation, J. Geophys. Res., 110, D20307, doi:10.1029/2005JD006240, 2005.

ACPD
14, 4051–4087, 2014

Liu, X., Chance, K., Sioris, C. E., and Kurosu, T. P.: Impact of using different ozone cross sections on ozone profile retrievals from Global Ozone Monitoring Experiment (GOME) ultraviolet measurements, Atmos. Chem. Phys., 7, 3571–3578, doi:10.5194/acp-7-3571-2007, 2007.

Liu, X., Bhartia, P. K., Chance, K., Spurr, R. J. D., and Kurosu, T. P.: Ozone profile retrievals from the Ozone Monitoring Instrument, Atmos. Chem. Phys., 10, 2521–2537, doi:10.5194/acp-10-2521-2010, 2010a.

Liu, X., Bhartia, P. K., Chance, K., Froidevaux, L., Spurr, R. J. D., and Kurosu, T. P.: Validation of Ozone Monitoring Instrument (OMI) ozone profiles and stratospheric ozone columns with Microwave Limb Sounder (MLS) measurements, Atmos. Chem. Phys., 10, 2539–2549, doi:10.5194/acp-10-2539-2010, 2010b.

McPeters, R. D., Labow, G. J., and Logan, J. A.: Ozone climatological profiles for satellite retrieval algorithms, J. Geophys. Res., 112, D05308, doi:10.1029/2005JD006823, 2007.

McPeters, R. D., Kroon, M., Labow, G., Brinksma, E. J., Balis, D., Petropavlovskikh, I., Veefkind, J. P., Bhartia, P. K., and Levelt, P. F.: Validation of the Aura ozone monitoring instrument total column ozone product, J. Geophys. Res., 113, D15S14, doi:10.1029/2007JD008802, 2008.

Petropavlovskikh, I., Evans, R., McConville, G., Oltmans, S., Quincy, D., Lantz, K., Disterhoft, P., Stanek, M., and Flynn, L.: Sensitivity of Dobson and Brewer Umkehr ozone profile retrievals to ozone cross-sections and stray light effects, Atmos. Meas. Tech., 4, 1841–1853, doi:10.5194/amt-4-1841-2011, 2011.

Pittman, J. V., Pan, L. L., Wei, J. C., Irion, F. W., Liu, X., Maddy, E. S., Barnet, C. D., Chance, K., and Gao, R.-S.: Evaluation of AIRS, IASI, and OMI ozone profile retrievals in the extratropical tropopause region using in situ aircraft measurements, J. Geophys. Res., 114, D24109, doi:10.1029/2009JD012493, 2009.

Rodgers, C. D.: Inverse Methods for Atmospheric Sounding: Theory and Practice, World Scientific Publishing, Singapore, 2000.

Scarnato, B., Staehelin, J., Stübi, R., and Schill, H.: Long-term total ozone observations at Arosa (Switzerland) with Dobson and Brewer instruments (1988–2007), J. Geophys. Res., 115, D13306, doi:10.1029/2009JD011908, 2010.

Schneider, M., Redondas, A., Hase, F., Guirado, C., Blumenstock, T., and Cuevas, E.: Comparison of ground-based Brewer and FTIR total column O_3 monitoring techniques, Atmos. Chem. Phys., 8, 5535–5550, doi:10.5194/acp-8-5535-2008, 2008.

ACPD
14, 4051–4087, 2014

van Oss, R. F., Voors, R. H. M., and Spurr, R. J. D.: Ozone profile algorithm, in: OMI Algorithm Theoretical Basis Document, vol. II, OMI Ozone Products, edited by: Bhartia, P. K., NASA Goddard Space Flight Cent., Greenbelt, Md, 51–73, 2001.
Veefkind, J. P., De Haan, J. F., Brinksma, E. J., Kroon, M., and Levelt, P. F.: Total ozone from the Ozone Monitoring Instrument (OMI) using the DOAS technique, IEEE T. Geosci. Remote, 44, 1239–1244, doi:10.1109/TGRS.2006.871204, 2006.
Wang, L., Newchurch, M. J., Biazar, A., Liu, X., Kuang, S., Khan, M., and Chance, K.: Evaluating AURA/OMI ozone profiles using ozonesonde data and EPA surface measurements for August 2006, Atmos. Environ., 45, 5523–5530., doi:10.1016/j.atmosenv.2011.06.012, 2011.
Weber, M., Lamsal, L. N., Coldewey-Egbers, M., Bramstedt, K., and Burrows, J. P.: Pole-to-pole validation of GOME WFDOAS total ozone with groundbased data, Atmos. Chem. Phys., 5, 1341–1355, doi:10.5194/acp-5-1341-2005, 2005.

ACPD
14, 4051–4087, 2014

Table 1. Brewer stations selected from WOUDC.

WMO ID	Station Name	Latitude, degree	Longitude, degree	Elevation, km	# of days[b]	Country
322	Petaling Jaya	3.1	101.64	0.05	1297	MYS
435	Paramaribo[a]	5.81	−55.21	0.01	1171	SUR
30	Marcus Island	24.29	153.98	0.01	1322	JPN
376	Mersa Matruh	31.33	27.22	0.04	1408	EGY
332	Pohang	36.03	129.38	0.01	1096	KOR
295	Mt. Waliguan	36.29	100.9	3.82	1331	CHN
213	El Arenosillo[a]	37.1	−6.73	0.04	1320	ESP
252	Seoul	37.57	126.95	0.08	1024	KOR
346	Murcia	38	−1.16	0.07	1320	ESP
447	Goddard[a]	38.99	−76.83	0.1	1065	USA
308	Madrid	40.45	−3.72	0.68	1293	ESP
261	Thessaloniki	40.52	22.97	0.05	1170	GRC
411	Zaragoza	41.63	−0.88	0.26	1253	ESP
305	Rome	41.9	12.5	0.08	1146	ITA
405	La Coruna	43.33	−8.41	0.06	1182	ESP
65	Toronto	43.78	−79.47	0.2	1227	CAN
326	Longfengshan	44.73	127.58	0.33	1287	CHN
35	Arosa	46.78	9.68	1.84	1242	CHE
100	Budapest	47.43	19.18	0.14	984	HUN
99	Hohenpeissenberg	47.81	11.01	0.98	1227	DEU
290	Saturna	48.78	−123.13	0.18	1119	CAN
331	Poprad-ganovce	49.03	20.32	0.71	1181	SVK
53	Uccle[a]	50.8	4.35	0.1	980	BEL
53	Uccle	50.8	4.35	0.1	1069	BEL
318	Valentia	51.93	−10.25	0.01	1027	IRL
316	De Bilt[a]	52.1	5.18	0.02	1153	NLD
76	Goose Bay	53.19	−60.23	0.04	1029	CAN
21	Edmonton	53.55	−114.1	0.77	1102	CAN
481	Tomsk	56.48	85.07	0.17	854	RUS
279	Norrkoping[a]	58.58	16.15	0.04	946	SWE
77	Churchill	58.74	−94.07	0.04	830	CAN
284	Vindeln	64.24	19.77	0.23	834	SWE
267	Sondrestrom	67	−50.62	0.3	719	GRL
262	Sodankyla	67.37	26.63	0.18	719	FIN
315	Eureka	79.99	−85.94	0.01	555	CAN
18	Alert	82.45	−62.51	0.06	525	CAN

[a] Stations with double Brewer monochromator. All other stations have single Brewer monochromator. Uccle (ID=53) provides both double and single Brewer measurements.
[b] The number of daily Direct Sun observations during the period 2005 to 2008.

ACPD
14, 4051–4087, 2014

Table 2. Comparison statistics* between OMI and Brewer total column ozone data for Northern Hemisphere (NH), mid-latitude, and high-latitude.

	NH: 24° N–79° N	Mid: 31° N–50° N	High: 51° N–79° N
SOE	0.04 ± 5.98 DU	−0.10 ± 5.84 DU	0.22 ± 6.33 DU
Mean bias ± 1σ	(0.02 ± 1.81 %)	(−0.02 ± 1.79 %)	(0.07 ± 1.88 %)
R	0.99	0.99	0.99
Regression	1.00 × +1.47 DU	0.99 × +2.38 DU	1.00 × −0.03 DU
TOMS	−5.52 ± 6.01 DU	−5.61 ± 5.72 DU	−5.57 ± 6.83 DU
Mean bias ± 1σ	(−1.7 ± 1.82 %)	(−1.75 ± 1.76 %)	(−1.65 ± 2.00 %)
R	0.99	0.99	0.99
Regression	0.99 × −3.19 DU	0.99 × −2.50 DU	0.99 × −3.43 DU
DOAS	−5.13 ± 7.14 DU	−5.67 ± 7.01 DU	−4.01 ± 7.64 DU
Mean bias ± 1σ	(−1.59 ± 2.18 %)	(−1.78 ± 2.16 %)	(−1.22 ± 2.24 %)
R	0.99	0.98	0.99
Regression	1.01 × −8.34 DU	1.00 × −6.33 DU	1.01 × −9.29 DU
KOE	9.15 ± 8.71 DU	7.29 ± 8.10 DU	12.74 ± 8.96 DU
Mean bias ± 1σ	(2.76 ± 2.60 %)	(2.23 ± 2.47 %)	(3.75 ± 2.60 %)
R	0.98	0.98	0.98
regression	1.03 × −1.49 DU	1.03 × −1.83 DU	1.01 × 8.51 DU

* Mean biases and 1σ standard deviations are in both DU and %. Correlation coefficients (R), slope and offset are from the linear regression.

ACPD
14, 4051–4087, 2014

Table 3. Correlations (R) between OMI-Brewer monthly mean total ozone differences of the four products (1–4th rows) and monthly solar zenith angle (5th row).

	31° N ≤ Latitude ≤ 38° N					40° N ≤ Latitude ≤ 49° N			
	SOE diff.	DOAS diff.	KOE diff.	TOMS diff.		SOE diff.	DOAS diff.	KOE diff.	TOMS diff.
SOE diff.	1				SOE diff.	1			
DOAS diff.	0.89	1			DOAS diff.	0.7	1		
KOE diff.	0.07	0.03	1		KOE diff.	0.03	0.10	1	
TOMS diff.	0.74	0.77	0.45	1	TOMS diff.	0.04	0.23	0.75	1
SZA	0.41	0.42	−0.81	−0.00	SZA	0.54	0.31	−0.66	−0.65

	50° N ≤ Latitude ≤ 58° N					64° N ≤ Latitude ≤ 79° N			
	SOE diff.	DOAS diff.	KOE diff.	TOMS diff.		SOE diff.	DOAS diff.	KOE diff.	TOMS diff.
SOE diff.	1				SOE diff.	1			
DOAS diff.	0.82	1			DOAS diff.	0.85	1		
KOE diff.	0.44	0.32	1		KOE diff.	−0.04	−0.31	1	
TOMS diff.	0.23	0.25	0.36	1	TOMS diff.	0.32	0.24	0.19	1
SZA	0.51	0.44	0.11	−0.54	SZA	0.7	0.54	0.03	−0.04

ACPD
14, 4051–4087, 2014

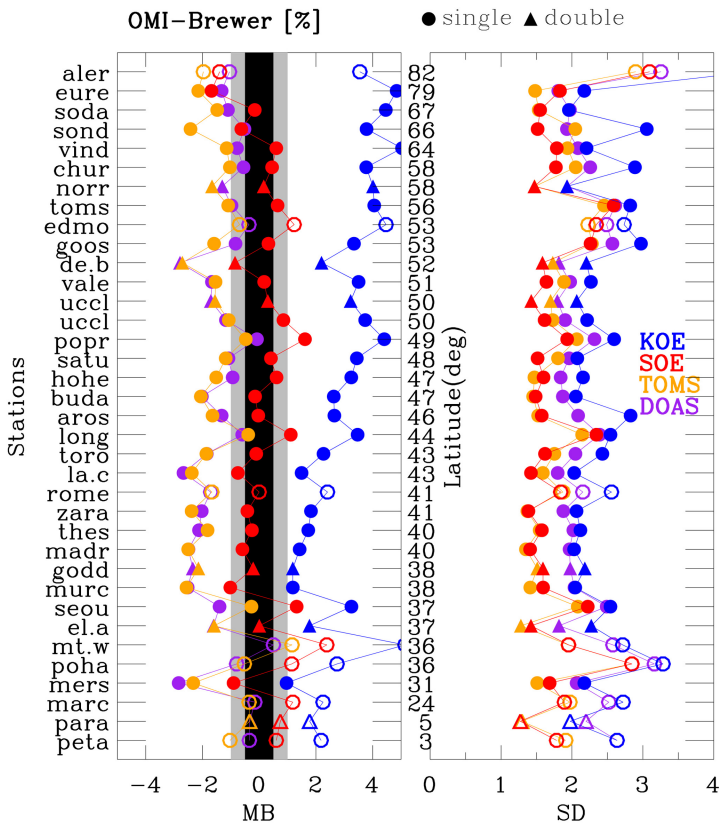

Fig. 1. Mean biases and 1σ standard deviations comparing OMI and Brewer total column ozone at the 36 Brewer stations listed in Table 1. The different color coding indicates the comparisons for four total column ozone data sets derived through KOE, SOE, TOMS, and DOAS algorithms, respectively. The circle and triangle symbols indicate single and double Brewer stations, respectively. The filled and opened symbols represent stations selected and rejected, respectively.

ACPD
14, 4051–4087, 2014

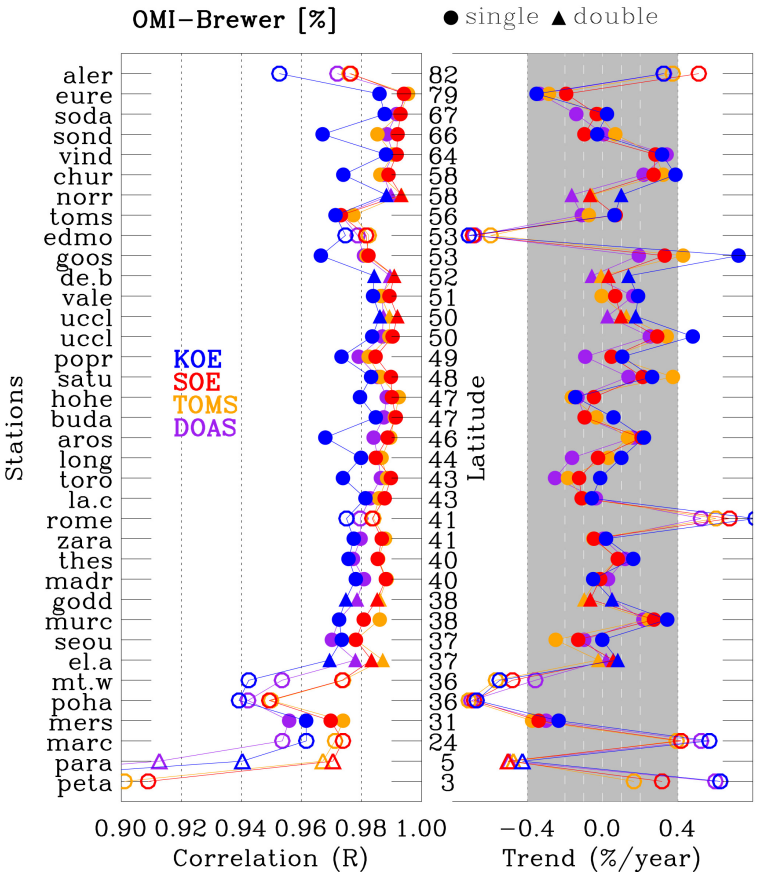

Fig. 2. Same as Fig. 1, but for correlation coefficient (R) and trends (%yr^{-1}). The correlation coefficient is calculated between OMI and Brewer total ozone columns. The trend is derived from the linear regression of the monthly differences between OMI and Brewer total ozone columns.

ACPD
14, 4051–4087, 2014

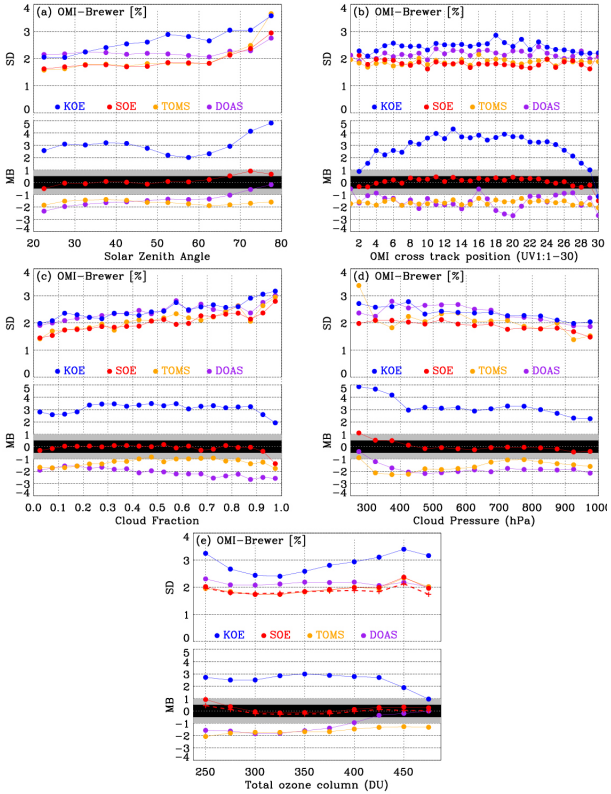

Fig. 3. Dependence of OMI-Brewer relative mean differences and 1σ standard deviations on (a) OMI solar zenith angle, (b) OMI cross-track position (UV1-based), (c) effective cloud fraction, (d) effective cloud-top pressure, and (e) total ozone column. The calculations for (c) and (d) are done for correlated data sets with OMI solar zenith angle $< 45^{\circ}$, in order to enhance the effect of cloud parameters on OMI retrievals. The red dashed line in Fig. 3e represents the SOE comparison with the use of the tropopause-dependent climatology presented in Bak et al. (2013).

ACPD
14, 4051–4087, 2014

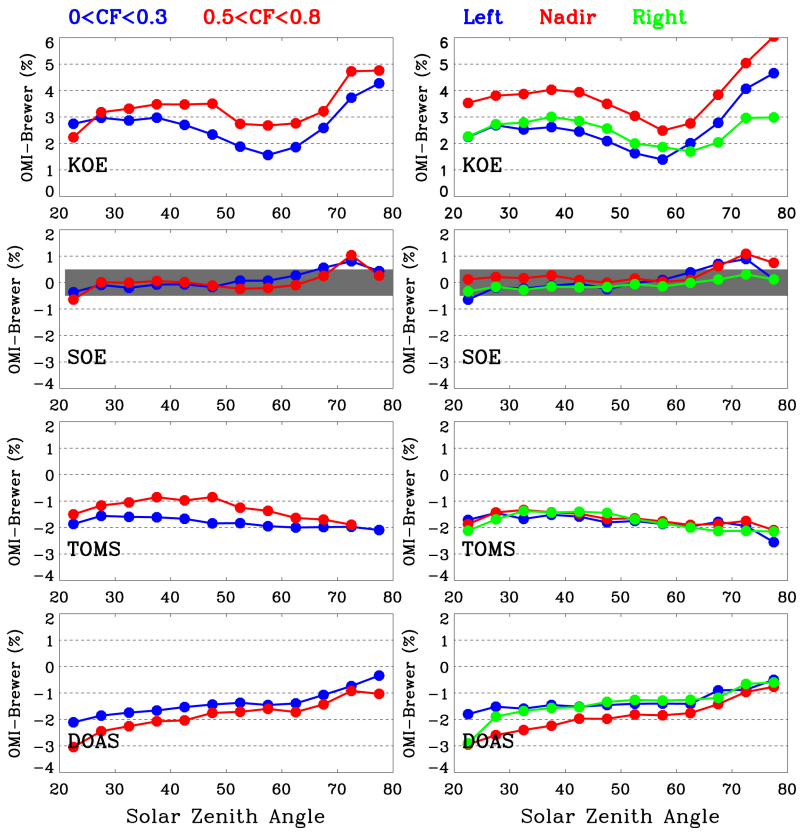

Fig. 4. Dependence of OMI-Brewer relative differences on solar zenith angle for (right panel) two groups of cloud fractions and for (left panel) three groups of OMI cross-track positions in UV-1 (Left side of the positions: 1–10, Nadir: 11–20, Right: 21–30).

ACPD
14, 4051–4087, 2014

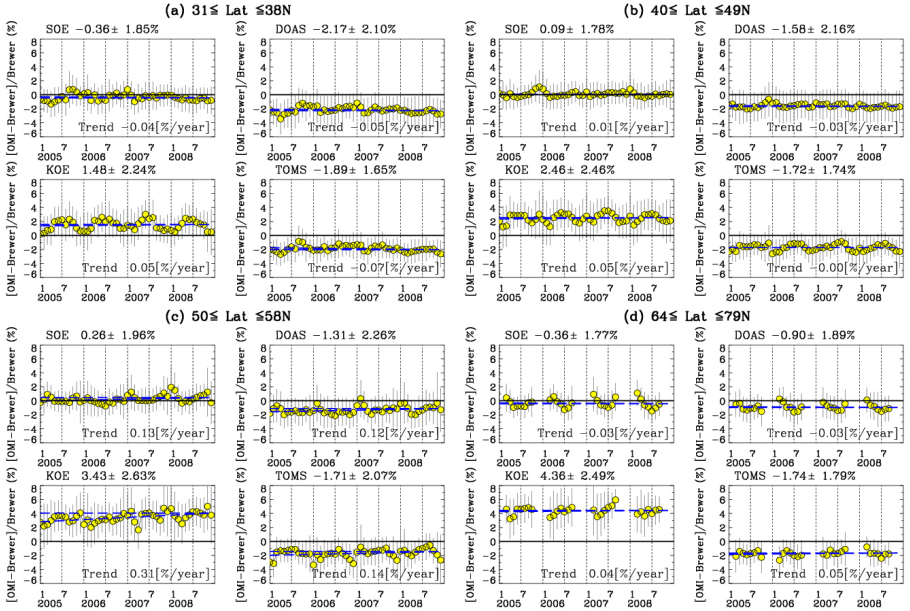

Fig. 5. Time series (monthly) of relative differences (yellow circles) between OMI and Brewer total ozone columns over four selected latitude bands and the 1σ standard deviations (vertical bars). The blue dashed line indicates a linear regression line with the linear trend shown at the bottom of each panel. The title of each panel indicates the overall mean bias and standard deviation.

ACPD
14, 4051–4087, 2014

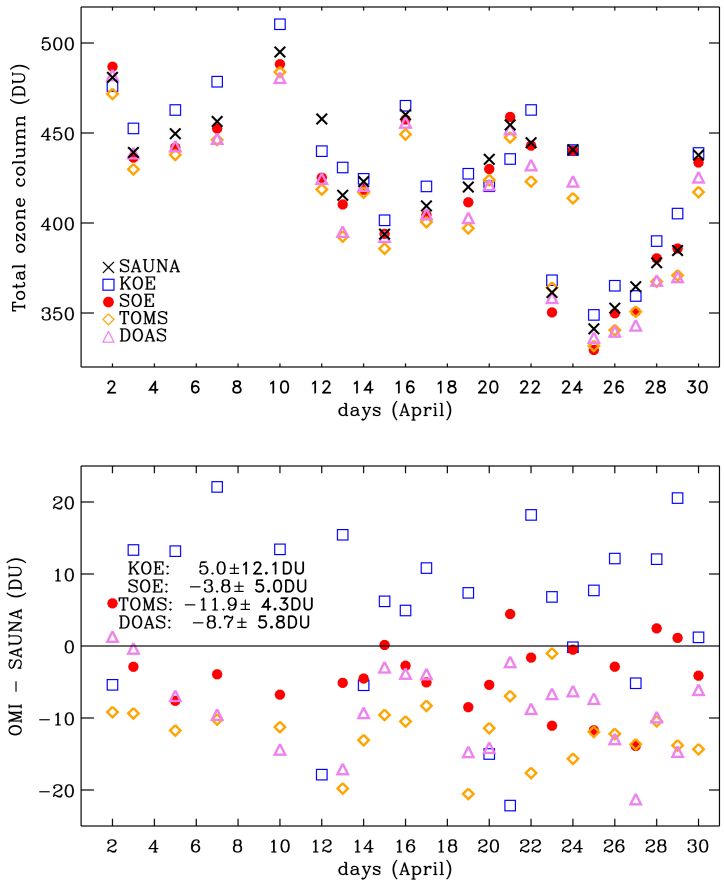

Fig. 6. (Upper) Time series of SAUNA data (Brewer reference) and OMI total column ozone for April 2006. (Lower) Time series of the relative differences between OMI and SAUNA total ozone.

ACPD
14, 4051–4087, 2014

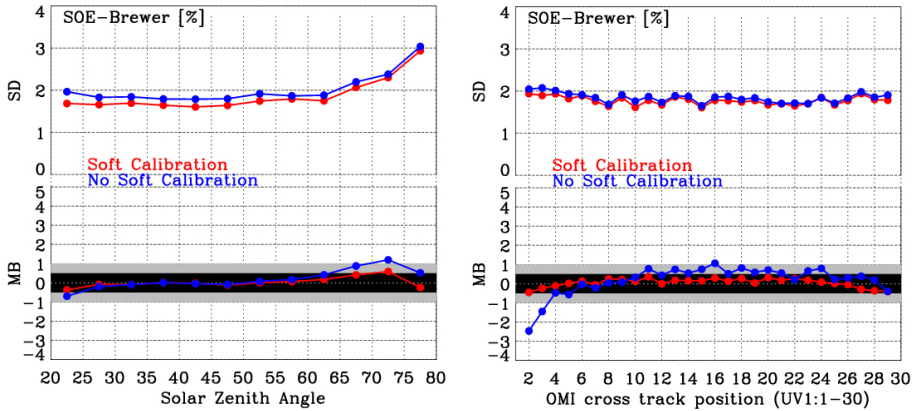

Fig. 7. Comparison between the SOE and Brewer total ozone columns with and without soft calibration as a function of solar zenith angle (left) and cross-track position (right).

ACPD
14, 4051–4087, 2014

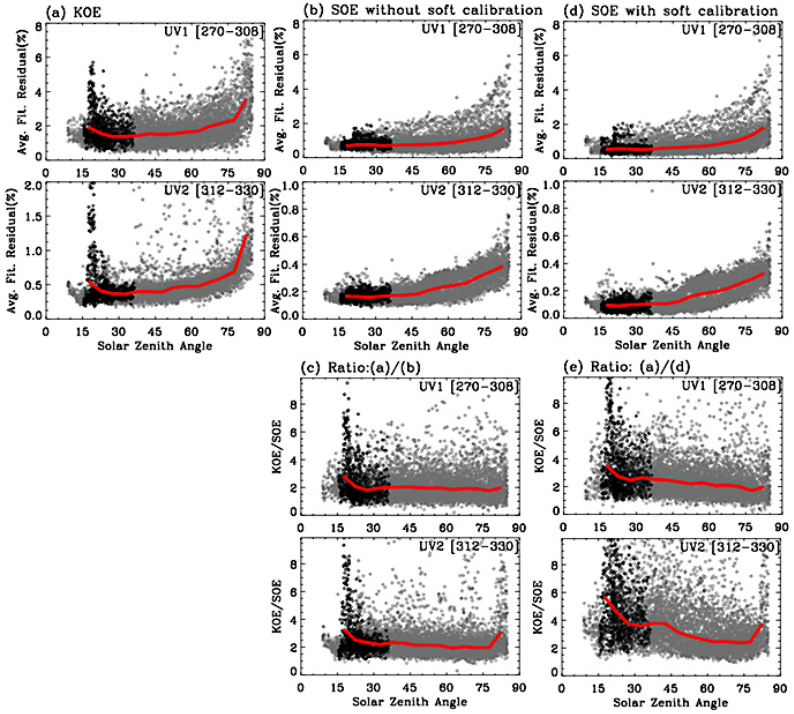

Fig. 8. Average fitting residuals in UV-1 and UV-2 channels for an orbit of retrievals (orbit 09987) on 1 June 2006 using **(a)** KOE, **(b)** SOE without soft calibration, and **(d)** SOE with soft calibration, as a function of solar zenith angle, with **(c, e)** the ratio of KOE to SOE fitting results. The average fitting residuals are defined as $\sqrt{\frac{1}{n}\sum_{i}^{n}\left(\frac{Y_{\text{measured from OMI}}-Y_{\text{calculated fromRTM}}}{Y_{\text{measured from OMI}}}\right)^2}\times 100\,\%$, n = # of wavelengths. The wavelengths are 270, 272.5, 274.7, 280.1, 282.5, 285.1, 287.0, 288.1, 290, 295, 300, 305, 308 nm in UV-1 channel and 312, 313, 315, 317.5, 320, 322.5, 325, 327.5, 330 nm in UV-2 channel, corresponding to outputs of KOE. The sun-glint contaminated pixels are indicated by the black symbol. The red line indicates the average in 5° SZA bins.

ACPD
14, 4051–4087, 2014